J. Hydrau., Coast. Environ. Eng., JSCE, No. 635/II-49, 141-152, 1999 November

MOTION OF DENSE FLUID RELEASED INTO QUIESCENT WATER WITH FINITE DEPTH

Xinya YING[1], Juichiro AKIYAMA[2] and Masaru URA[3]

[1] Student Member of JSCE, Graduate Student, Graduate School of Engineering, Kyushu Institute of Technology (1-1 Sensuicho, Tobataku, Kitakyushu 804-8550, Japan)

[2] Member of JSCE, Associate Professor, Dept. of Civil Engineering, Kyushu Institute of Technology

[3] Member of JSCE, Professor, Dept. of Civil Engineering, Kyushu Institute of Technology

The motion of a 2-D heavy turbulent thermal as well as a horizontally propagating density flow subsequently formed after impinging on the bottom is studied by large eddy simulations (LES). The governing equations, which consist of the filtered 2-D Navier-Stokes equations and mass conservation equation, are solved using the combined cubic spline (CCS) scheme. The eddy viscosity is evaluated by the Smagorinsky model.

The comparisons of computational results with experimental results show that the motion of both falling and horizontal propagating stage is well simulated by the present numerical model. The added mass coefficient A_m for the thermal is estimated as 0.6, based on numerical simulation. The good agreements between experimental, computed and theoretical results of half width, average buoyancy and mass center velocity of the thermal are achieved. The numerical experiment reveals that motion of the thermal is dependent on the initial volume of dense fluid, even if initial buoyancy remains constant.

Key Words *: thermals, density current, LES, Smagorinsky model, CCS scheme*

1. INTRODUCTION

When a dense fluid is instantaneously released into a less dense fluid with finite depth, the dense fluid freely falls and spreads under the action of its own buoyancy during falling stage, which are commonly referred to as a heavy turbulent thermal. After impinging on the bottom, it splits into two clouds and each one propagates horizontally along the bottom (see **Fig.1**). A practical example of the considered flow is dumping sludge or soil into coastal waters using bottom-dump barges, which is often encountered in construction of man-made islands etc. It is of practical importance to predict the flow for assessing the environmental impact on plankton and benthic organism near disposal site.

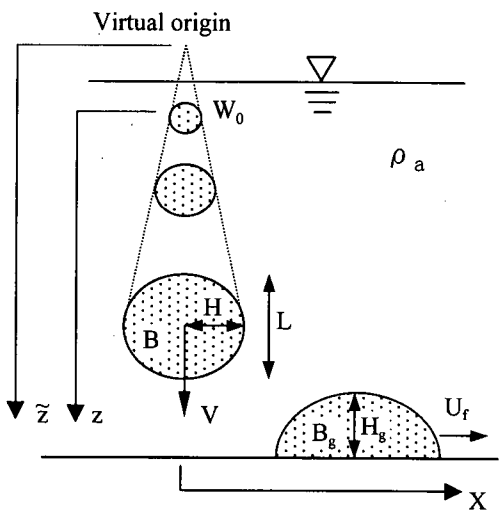

Fig.1 Sketch of the motion of 2-D dense cloud

To understand the flow characteristics of the thermal, a great deal of study has been performed. For instance, Scorer[1)] obtained empirical equations on the width and the front position of the thermal. Wang[2)] developed a model for the motion of a turbulent buoyant thermal in a calm, stably stratified atmosphere, based on the conservation of mass, momentum and enthalpy. Using this model, the average motion of the thermal is described in terms of its initial density difference, velocity and effective radius as well as mass entrainment constant, effective drag coefficient and turbulent

dissipation rate. However, the added mass is ignored in this model. In addition, the model was not verified by experimental data. Escudier and Maxworthy[3] proposed a model to describe the average motion of the thermal based on the conservation of momentum and mass. In this model, the added mass is included, while the drag force acted on the thermal body is ignored. Again, this model was not verified by experimental data. Baines and Hopfinger[4] investigated experimentally and theoretically the motion of the thermal with large density difference. They found that the effects of large density difference are confined to the region close to the source. Akiyama et al.[5] conducted a series of experiment on 2-D heavy turbulent thermals and developed a thermal model to predict such flow characteristics as half width, velocity and average buoyancy. In this model, both added mass and drag force are included. The entrainment coefficient and the drag coefficient are quantified based on a large number of experimental data. Nakatsuji et al.[6] made a theoretical and experimental study on particle thermals, which are formed by an instantaneous release of particles into water. They found experimentally that the average motion of the particle thermal is close to that of the thermal formed by dense fluid if the initial volume of cloud is relatively large and the size of particles is relatively small. As to the horizontal propagation stage after impinging on the bottom, Tamai et al.[7] conducted experimental and theoretical investigations.

The aforementioned thermal models are essentially based on similarity in thermal shape. Such analyses are useful to understand the fundamentals of the motion of the thermal in a fully developed state. However, heavy turbulent thermals in practice take place in complicated conditions, such as the presence of a density gradient, the occurrence of a current, the limitation of ambient water depth and others. It necessitates development of a numerical model. For instance, Li[8] studied particle thermals experimentally and numerically employing a mixing length model, and found that the velocity of the thermal approaches the terminal settling velocity of the individual particles and the growth rate of half width of thermal decreases with the magnitude of the settling velocity of particles. Tamai and Muraoka[9] investigated qualitatively turbidity transport produced by direct dumping of soil using the two-fluid k- ε turbulence model. They found that the induced flow is depressed by slowing down the dump of soil. Oda et al.[10] investigated settling and spreading behavior of particle cloud using the improved DEMAC method.

In the present work, an attempt is made to develop a numerical model to simulate a 2-D heavy turbulent thermal using the large eddy simulation (LES). Although turbulence is physically three-dimensional, two-dimensional simulations are often used as an approximate approach in many researches (e.g. Paolucci 1990[11], Tafti and Vanka 1991[12], Fang et al. 1997[13]). All of these studies have shown that two-dimensional simulations are able to give good predictions in many situations in which mean flows are two-dimensional.

The governing equations are solved using the newly developed the combined cubic spline (CCS) scheme. The validity of the model is extensively tested against experimental data for the whole process of the motion of a dense cloud from falling to horizontal propagation stage. This work is the first stage of our final objective to simulate the practical case of dumping dredged material in coastal waters and lakes.

2. MODEL FORMULATION

Applying grid filter to the 2-D incompressible Navier-Stokes equations as well as the equation of conservation of mass, we can obtain the following governing equations

$$\frac{\partial U_i}{\partial x_i} = 0 \tag{1}$$

$$\frac{\partial U_i}{\partial t} + U_j \frac{\partial U_i}{\partial x_j} = -\frac{1}{\rho}\frac{\partial P}{\partial x_i} + \nu \frac{\partial^2 U_i}{\partial x_j^2} + \frac{\partial}{\partial x_j}\left(-\overline{u_i' u_j'}\right) + g_i \frac{\Delta \rho}{\rho} \tag{2}$$

$$\frac{\partial \Delta \rho}{\partial t} + U_i \frac{\partial \Delta \rho}{\partial x_i} = \frac{\partial}{\partial x_i}\left(-\overline{u_i' \Delta \rho'}\right) \tag{3}$$

where U_i is the large-scale quantities of velocity component in the direction x_i; P the large-scale pressure minus the hydrostatic pressure at reference density ρ_a; ρ the large-scale density; $\Delta \rho$ the density excess ($= \rho - \rho_a$); g_i the specific body force in the direction x_i; $u_i', \Delta \rho'$ the fluctuating velocity and density excess. $\overline{u_i' u_j'}$ the correlation terms between fluctuating velocity due to space averaging. By using eddy viscosity concept, the correlation terms take the form

$$-\overline{u_i' u_j'} = \nu_t \left(\frac{\partial U_i}{\partial x_j} + \frac{\partial U_j}{\partial x_i} \right) - \frac{2}{3} k \delta_{ij} \tag{4}$$

where ν_t is the subgrid scale eddy viscosity; k the turbulent kinetic energy ; δ_{ij} the Kronecker delta function. The last term in the right-hand side of Eq.(4) represents the normal stresses and can be

absorbed in the pressure terms of the momentum equations.

By assuming that subgrid turbulent production includes buoyancy effects[14], ν_t is expressed as

$$\nu_t = (Cs\Delta)^2\left(|\bar{S}|^2 - \frac{g_i}{\rho Scs}\frac{\partial \Delta\rho}{\partial x_i}\right)^{1/2} \quad (5)$$

where Δ is the filter width, Cs the Smagorinsky constant, and $|\bar{S}| = (2\bar{S}_{ij}\bar{S}_{ij})^{1/2}$ the magnitude of large-scale strain rate tensor in which $\bar{S}_{ij}$ is defined by

$$\bar{S}_{ij} = \frac{1}{2}\left(\frac{\partial U_i}{\partial x_j} + \frac{\partial U_j}{\partial x_i}\right) \quad (6)$$

The term $-\overline{u_i'\Delta\rho'}$ in Eq. (3) is generally assumed to be

$$-\overline{u_i'\Delta\rho'} = \frac{\nu_t}{Scs}\frac{\partial \Delta\rho}{\partial x_i} \quad (7)$$

where Scs is the subgrid turbulent Schmidt number and is defined as the ratio of eddy diffusivity of momentum to eddy diffusivity of matter.

Using the operator-splitting algorithm[15),16)], the governing equations for flow, namely, Eqs. (1) and (2) are divided into the following two steps:

1) Advection and Diffusion

$$\frac{\partial U_i}{\partial t} + U_j\frac{\partial U_i}{\partial x_j} = \nu\frac{\partial^2 U_i}{\partial x_j^2} + \frac{\partial}{\partial x_j}\left(\nu_t\left(\frac{\partial U_i}{\partial x_j} + \frac{\partial U_j}{\partial x_i}\right)\right)$$

$$[n\Delta t \le t \le (n+\frac{1}{2})\Delta t] \quad (8)$$

2) Pressure

$$\frac{\partial U_i}{\partial x_i} = 0 \quad (9)$$

$$\frac{\partial U_i}{\partial t} = -\frac{1}{\rho}\frac{\partial P}{\partial x_i} + g_i\frac{\Delta\rho}{\rho}$$

$$[(n+\frac{1}{2})\Delta t \le t \le (n+1)\Delta t] \quad (10)$$

The pressure is obtained by solving the Poisson type equation deduced from the algebraic manipulation of Eqs.(9) and (10). The density excess and velocity are obtained by solving Eqs. (3) and (8) using the combined cubic spline (CCS) scheme. The CCS scheme for 2-D advection and diffusion problems is described as follows.

The 2-D advection and diffusion equation can be expressed in the form

$$\frac{\partial f}{\partial t} + u\frac{\partial f}{\partial x} + v\frac{\partial f}{\partial y} = D\frac{\partial^2 f}{\partial x^2} + D\frac{\partial^2 f}{\partial y^2} \quad (11)$$

where f is a scalar, u and v are velocity component in x and y direction, and D is a diffusion coefficient.

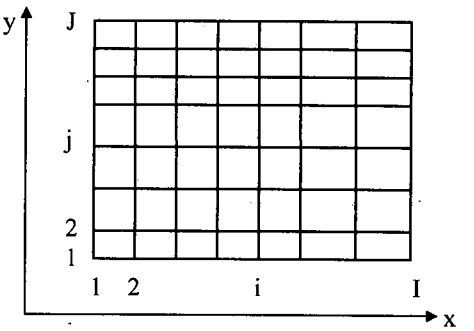

Fig.2 Sketch of mesh for 2-D CCS scheme

If the time derivatives are expressed by a combined algorithm, and the spatial distribution of scalar f is fitted by a series of cubic spline passing through grid points $\{x_1,y_j\},\{x_2,y_j\},....,\{x_I,y_j\}$, j=1, 2,$\cdots$, J for x-direction and $\{x_i,y_1\},\{x_i,y_2\},....,\{x_i,y_J\}$, i=1, 2,$\cdots$, I for y-direction (see **Fig.2**), Eq. (11) is transformed to

$$\frac{f_{i,j}^{n+1} - f_{i,j}^{n}}{\Delta t} = \theta\,(D_{i,j}^{n}Mx_{i,j}^{n} + D_{i,j}^{n}My_{i,j}^{n} - u_{i,j}^{n}Nx_{i,j}^{n} - v_{i,j}^{n}Ny_{i,j}^{n}) + (1-\theta)(D_{i,j}^{n+1}Mx_{i,j}^{n+1} + D_{i,j}^{n+1}My_{i,j}^{n+1} - u_{i,j}^{n+1}Nx_{i,j}^{n+1} - v_{i,j}^{n+1}Ny_{i,j}^{n+1}) \quad (12)$$

in which

$$Nx_{i,j}^{n} = \left.\frac{\partial f}{\partial x}\right|_{i,j}^{n} \qquad Mx_{i,j}^{n} = \left.\frac{\partial^2 f}{\partial x^2}\right|_{i,j}^{n}$$

$$Ny_{i,j}^{n} = \left.\frac{\partial f}{\partial y}\right|_{i,j}^{n} \qquad My_{i,j}^{n} = \left.\frac{\partial^2 f}{\partial y^2}\right|_{i,j}^{n}$$

θ is a weight coefficient ($0 \le \theta \le 1$), for explicit scheme $\theta = 1$, for fully implicit scheme $\theta = 0$, for the scheme similar to Crank-Nicolson $\theta = 0.5$. For the cubic spline interpolation passing through the grid points $\{x_1,y_j\},\{x_2,y_j\},.....,\{x_I,y_j\}$, we can obtain[17)]

$$\frac{\Delta x_{i-1}}{6}Mx_{i-1,j}^{n} + \frac{\Delta x_{i-1}+\Delta x_i}{3}Mx_{i,j}^{n} + \frac{\Delta x_i}{6}Mx_{i+1,j}^{n} = \frac{f_{i+1,j}^{n} - f_{i,j}^{n}}{\Delta x_i} - \frac{f_{i,j}^{n} - f_{i-1,j}^{n}}{\Delta x_{i-1}} \quad (i = 2, I-1) \quad (13)$$

in which $\Delta x_i = x_{i+1} - x_i$.

$Mx_{1,j}^{n}$ and $Mx_{I,j}^{n}$ are determined according to the boundary conditions. Then, $Mx_{i,j}^{n}(i = 2, I-1)$ can be determined by Eq. (13). $Nx_{i,j}^{n}(i = 1, I)$ is calculated by the equations

$$Nx_{1,j}^n = -\left(\frac{Mx_{1,j}^n}{3} + \frac{Mx_{2,j}^n}{6}\right)\Delta x_1 + \frac{f_{2,j}^n - f_{1,j}^n}{\Delta x_1} \quad (14)$$

$$Nx_{i,j}^n = \left(\frac{Mx_{i,j}^n}{3} + \frac{Mx_{i-1,j}^n}{6}\right)\Delta x_{i-1} + \frac{f_{i,j}^n - f_{i-1,j}^n}{\Delta x_{i-1}} \quad (i = 2, I) \quad (15)$$

Similarly, for the cubic spline interpolation passing through the grid points $\{x_i, y_1\}, \{x_i, y_2\}, \cdots, \{x_i, y_J\}$, we can obtain

$$\frac{\Delta y_{j-1}}{6} My_{i,j-1}^n + \frac{\Delta y_{j-1} + \Delta y_j}{3} My_{i,j}^n + \frac{\Delta y_j}{6} My_{i,j+1}^n = \frac{f_{i,j+1}^n - f_{i,j}^n}{\Delta y_j} - \frac{f_{i,j}^n - f_{i,j-1}^n}{\Delta y_{j-1}} \quad (j = 2, J-1) \quad (16)$$

in which $\Delta y_j = y_{j+1} - y_j$.

$My_{i,1}^n$ and $My_{i,J}^n$ are determined according to the boundary conditions. Then, $My_{i,j}^n (i = 2, I-1)$ can be determined by Eq. (16). $Ny_{i,j}^n (j = 1, J)$ is calculated by the equations

$$Ny_{i,1}^n = -\left(\frac{My_{i,1}^n}{3} + \frac{My_{i,2}^n}{6}\right)\Delta y_1 + \frac{f_{i,2}^n - f_{i,1}^n}{\Delta y_1} \quad (17)$$

$$Ny_{i,j}^n = \left(\frac{My_{i,j}^n}{3} + \frac{My_{i,j-1}^n}{6}\right)\Delta y_{j-1} + \frac{f_{i,j}^n - f_{i,j-1}^n}{\Delta y_{j-1}} \quad (j = 2, J) \quad (18)$$

Finally, $f_{i,j}^{n+1}$ ($i=1,2,\cdots,I$ and $j=1,2,\cdots,J$) are obtained by solving Eq.(12). If θ is not equal to 1, iteration technique is employed in solving Eq.(12). The comparisons between the CCS scheme and some conventional schemes show that the CCS scheme is almost free from numerical diffusion and numerical oscillation (see Appendix A). The CCS scheme has been found to be advantageous in solving the advection and diffusion equation because of its remarkable accuracy and simplicity as well as the ability to be easily extended to multi-dimensional problems.

3. THEORETICAL CONSIDERATIONS

The motion of turbulent thermal are theoretically investigated by Akiyama et al.[5], Baines and Hopfinger[4], Escudier and Maxworth[3], Wang[2] and others. The assumptions employed in these studies are essentially the same, namely:

(1) There is no loss of momentum and buoyancy from the thermal.

(2) The thermal does not change shape during the motion and all fluid and flow properties are uniformly distributed within it.

Herein, the thermal model developed by Akiyama et al.[5], which includes the added mass as well as drag force, is briefly described. Introducing two shape coefficients S_1 and S_2, area A and circumference length C of thermal are expressed as

$$A = 2S_1HL \quad (19)$$

$$C = S_2\sqrt{HL} \quad (20)$$

Assuming the shape of the thermal to be an ellipse, the shape factors S_1 and S_2 are given by

$$S_1 = \frac{\pi}{4} \quad (21)$$

$$S_2 = \pi\sqrt{\frac{4F^2+1}{2F}} \quad (22)$$

where F is the half width-to-length ratio (=H/L). Based on the conservation of volume, mass and momentum, A set of governing equations on a 2-D turbulent thermal[5] is given by

$$\frac{d}{dt}(2S_1HL) = q_e \quad (23)$$

$$\frac{d}{dt}(2S_1HLB) = 0 \quad (24)$$

$$\frac{d}{dt}\{2S_1HL(1+A_m)V\} = 2S_1HLB - 2C_dV^2H \quad (25)$$

where B is the average buoyancy ($= g(\overline{\rho} - \rho_a)/\rho_a$), $\overline{\rho}$ the average density of thermal, A_m the added mass coefficient and C_d the drag coefficient, q_e is the entrainment rate of ambient fluid into the thermal body and is expressed as

$$q_e = E_dS_2\sqrt{HL}V \quad (26)$$

where E_d is the entrainment coefficient.

Converting the variable of integration in the governing equations from time t to $\tilde{z}$ (the distance measured from the virtual origin, see **Fig.1**) and solving the equations, we obtain the following relationships[5]

$$H = \frac{E_d\sqrt{F}S_2\tilde{z}}{4S_1} \quad (27)$$

$$B = \frac{8S_1W_0}{E_d^2S_2^2\tilde{z}^2} \quad (28)$$

$$V = \sqrt{\left(\frac{\tilde{z}_i}{\tilde{z}}\right)^{\alpha}V_i^2 + \frac{\beta}{\alpha-1}\left(\frac{\tilde{z}^{\alpha-1} - \tilde{z}_i^{\alpha-1}}{\tilde{z}^{\alpha}}\right)} \quad (29)$$

in which W_0 is the initial total buoyancy ($= A_0g(\rho_0 - \rho_a)/\rho_a$), A_0 and ρ_0 is the initial volume per unit width and density of the source, respectively. V_i is the mass center velocity at arbitrary distance $\tilde{z}_i$. α and β are given by the following functions.

$$\alpha = 4\left\{1 + \frac{2\sqrt{FC_d}}{(1+A_m)E_d S_2}\right\} \quad (30)$$

$$\beta = \frac{16 S_1 W_0}{(1+A_m)E_d^2 S_2^2} \quad (31)$$

If a real source has initial half width of H_0, based on Eq.(27), distance from the virtual origin to center of real source is determined as

$$\tilde{z}_0 = \frac{4 S_1 H_0}{E_d \sqrt{F S_2}} \quad (32)$$

Thus, the relationship between $\tilde{z}$ and z (distance measured from center of real source) is expressed as

$$\tilde{z} = \tilde{z}_0 + z \quad (33)$$

If real source start from rest, namely, when $\tilde{z}_i = \tilde{z}_0$, V_i=0, Eq. (29) is rewritten as

$$V = \sqrt{\frac{\beta}{\alpha - 1}\left(\frac{\tilde{z}^{\alpha-1} - \tilde{z}_0^{\alpha-1}}{\tilde{z}^{\alpha}}\right)} \quad (34)$$

H, B and V of the thermal can be obtained from above equations. The values of coefficients F and E_d are determined as 0.6 and 0.4, respectively, based on the experimental studies by Akiyama et al.[5]. The value of A_m is set to equal to that of rigid ellipse cylinder, namely, A_m=2F, based on potential theory.

4. RESULTS

(1) Free fall stage

In order to verify the numerical model, the experiments on 2-D heavy turbulent thermals were performed in a glass flume of 7.5m length, 1.0m height and 0.1m width. A salt solution marked with fluorescence was used to produce the thermals. The dense fluid was released into quiescent water by a device that was placed just above the water surface. The initial volume per unit width of the thermal was A_0=0.005m^2. The initial total buoyancy W_0 was equal to 0.001764 m^3/s^2 for CASE1 and 0.0098 m^3/s^2 for CASE2. The motions of the dense clouds were imaged by a VTR-camera moving with the falling speed of the dense cloud. The velocity of mass center and the geometry of the cloud were obtained based on the analysis of the recorded images. Average buoyancy B was calculated by the initial total buoyancy divided with the area of the cloud.

In the computation, domain is a rectangle of 2.0m width and 1.4m height. All boundaries are considered as slip wall boundaries. The boundary conditions for velocity, pressure and density are

$$\frac{\partial V_\tau}{\partial n} = 0 \quad V_n = 0 \quad \frac{\partial P}{\partial n} = 0 \quad \frac{\partial \Delta\rho}{\partial n} = 0$$

where τ = direction tangential to boundary, and n = direction perpendicular to boundary.

Grid size is 0.01m×0.01m. The time step size is 0.025s for CASE1 and 0.01s for CASE2. The values of Cs and Scs are 0.16 and 0.1, that were determined by matching computational results and experimental results of inclined plumes[18].

Fig.3 shows experimental photographs of the thermal and computed velocity as well as density excess fields for CASE1. The computed thermal area is defined as $\Delta\rho/\rho > 10^{-6}$, which is determined such that the computed thermal area agree well with the experimental results. It is seen from this figure that shape, size and fall velocity of the thermal are well predicted by the computation. The shape of the thermal in experiment is slightly irregular because of the unsteady nature of the flow. The wake of the thermal appears in both computational and experimental results. However, the buoyancy loss to the wake of thermal is not significant to the motion of the thermal, because the buoyancy within the wake is found to be relatively small. For example, in the case as shown in **Fig.3**, the buoyancy loss to the wake is about 4% of the total buoyancy. This confirms that in the theoretical treatment for the conservative thermal the assumption that no buoyancy is lost to the wake of thermal is valid[5]. The shape of the thermal changes gradually from a circle to an ellipse with the half width-to-length ratio H/L of about 0.62 at t=10s in both experiment and computation. We also found that the velocity fields of two symmetrical vortex structures are established soon after release. The velocity fields reveal that the formation of wake is due to the velocity differences between the main part and the rear part of the thermal. Since velocity at the rear part is much smaller than the main part, the rear part is left behind as the main part moves forward. The maximum of velocity near the center of the thermal is about 3 times larger than mass center velocity V. During the early stages of the motion, the maximum of density excess appears near the center of cloud, and after some distance the phenomenon of double-peak distribution appears due to the entrainment of less dense fluid into the central part from the rear of the thermal.

From **Fig.3**, we also found that flow field around the thermal is somewhat different from that around a rigid ellipse cylinder with the same shape and size as the thermal. This indicates that the value of added mass coefficient A_m for the thermal can not be expressed by that of equivalent rigid ellipse cylinder. A_m is defined as the ratio of kinetic energy of added mass to that of the thermal, namely,

$$A_m = \iint_{OT} \frac{1}{2}\rho(U_1^2 + U_2^2)dxdy \Big/ \left(\frac{1}{2}M_T V^2\right) \quad (35)$$

where OT is the flow field outside the thermal, U_1

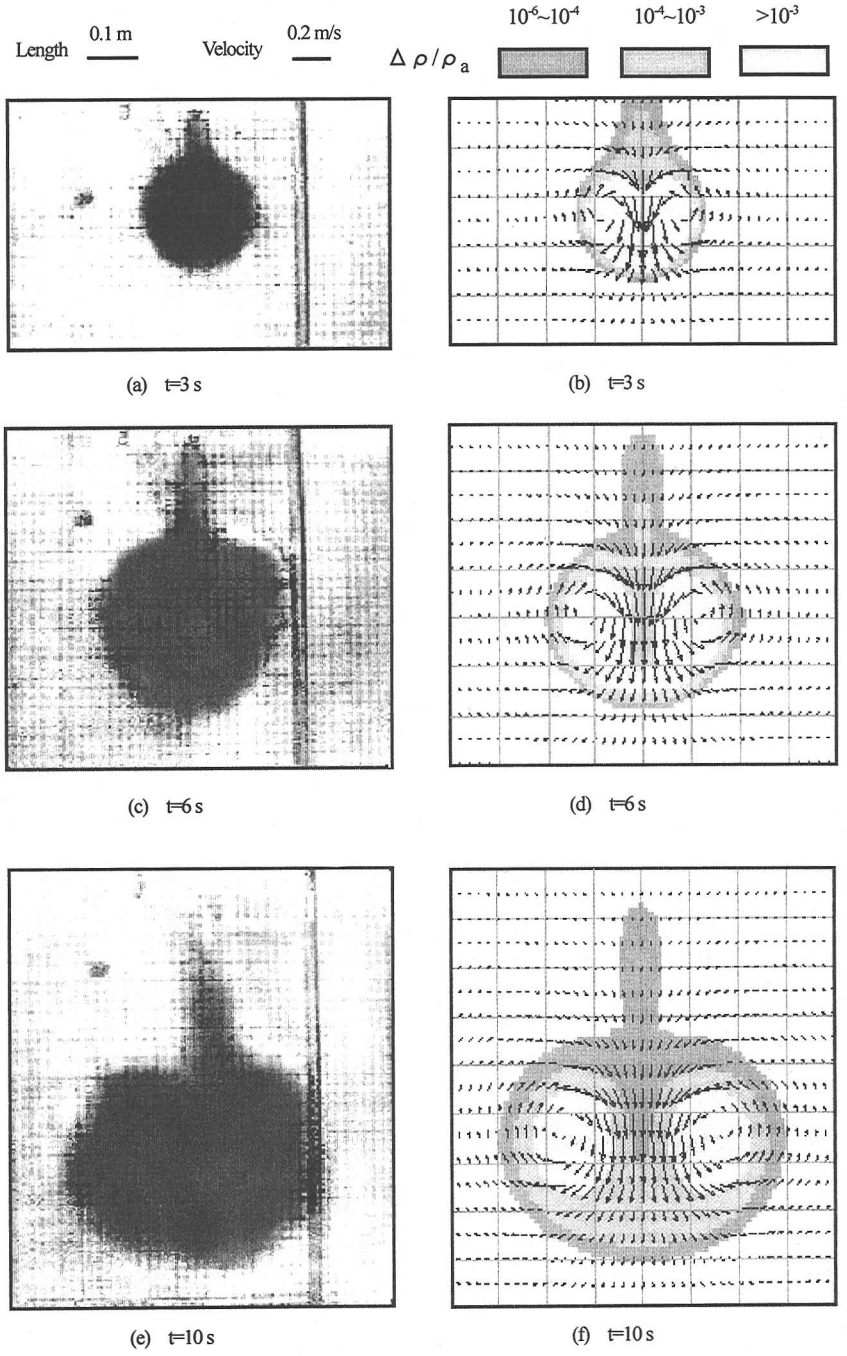

Fig.3 Photographs and computed velocity and density excess fields (CASE1)
(a),(c) and (e) are photographs; (b),(d) and (f) are computational results

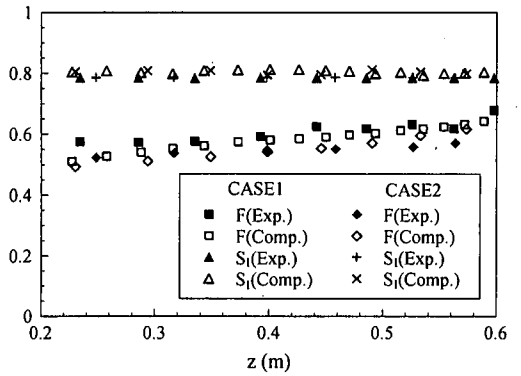

Fig.4 F and S_1 as functions of z

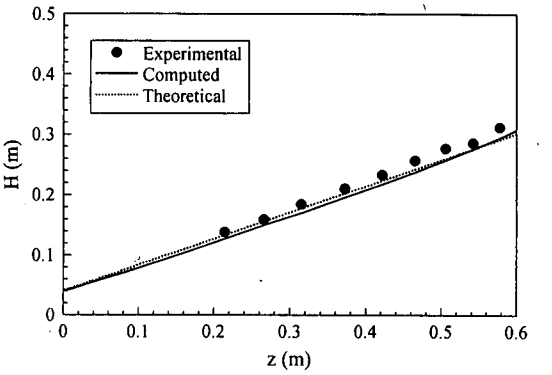

Fig.6 H as a function of z (CASE1)

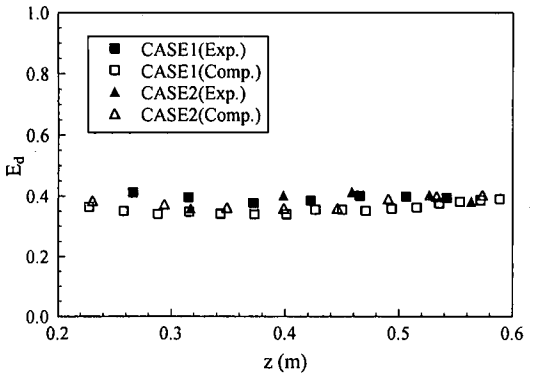

Fig.5 E_d as a function of z

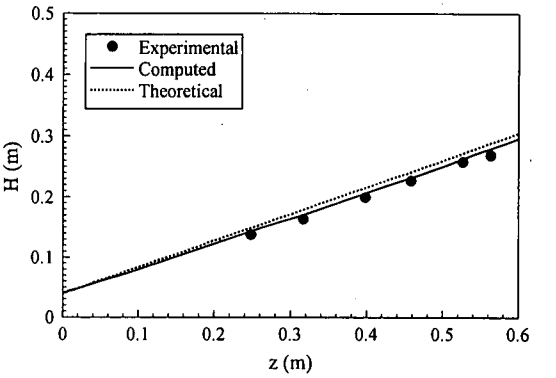

Fig.7 H as a function of z (CASE2)

and U_2 are velocity components in the direction x and y, respectively, and M_T is the total mass of thermal. Based on the numerical simulation, the value of A_m is estimated as 0.6, which is only half of the value estimated from the relationship for a rigid ellipse cylinder (A_m=2F).

In **Fig.4**, the half width-to-length ratio F and shape coefficient S_1 are plotted against z. It is found that S_1 is almost constant with z and average values of computed S_1 is about 0.8, which is very close to $\pi/4$ (the value of S_1 for an ellipse). The values of F tend to increase slightly with z and average value of F is about 0.6 for both experimental and computational results. No significant differences are found between the results of CASE1 and CASE2. Note that the experimental data used in this work are average results of five runs under the same experimental conditions.

From Eqs.(23) and (26), the entrainment coefficient Ed is expressed as

$$E_d = \frac{dA/dt}{S_2\sqrt{HLV}} \qquad (36)$$

The right hand side of Eq.(36) can be determined by both the experiment and numerical simulation. The experimental and computational results of E_d are presented in **Fig.5**. The computational results confirm that the value of E_d is nearly independent of z, which has been suggested by Akiyama et al.[5]. The average values of computed E_d are 0.36 (CASE1) and 0.38 (CASE2), which are close to 0.4 obtained by the experiment.

The above experimental and computed results have shown that for different W_0 no significant differences in the values of S_1, F, A_m and E_d are identified. This is because the thermals, even if W_0 is different, keep good similarities. This finding is further confirmed in the following comparisons between experimental, computed and theoretical results.

In **Figs.6 ~ 11**, the computed results of H, B and V are compared with the results obtained by the experiment and the thermal model[5] under the same initial total buoyancy W_0. In the thermal model, F=0.6, $S_1=\pi/4$, S_2=4.48, E_d=0.4 and A_m=0.6 are used. The value of C_d is determined as 0.8, according to Eq.(25) and related computational results.

Akiyama et al.[5] found that half width of the thermal H increases linearly with z and the value of growth rate dH/dz is around 0.48. Baines and Hopfinger[4] also found the linear relationship between H and z in their studies on light thermals.

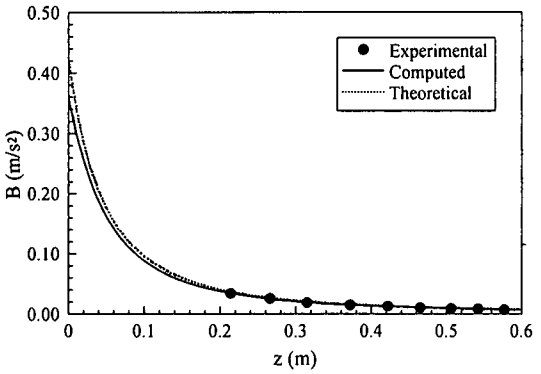

Fig.8 B as a function of z (CASE1)

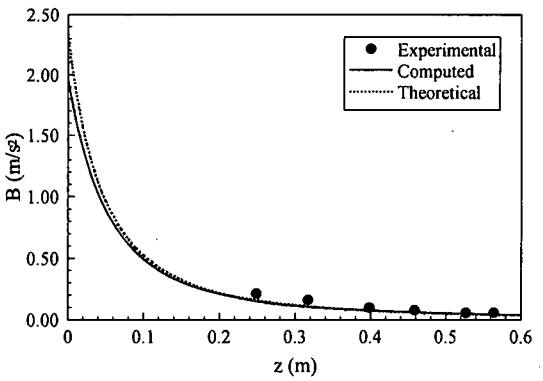

Fig.9 B as a function of z (CASE2)

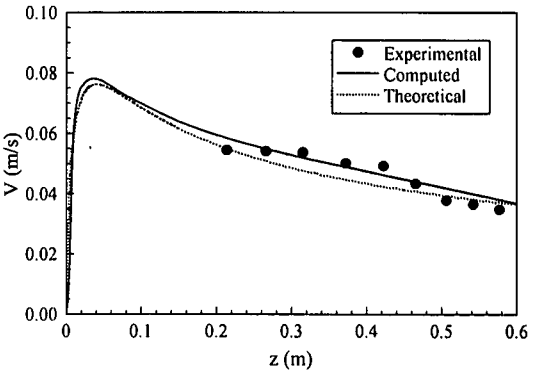

Fig.10 V as a function of z (CASE1)

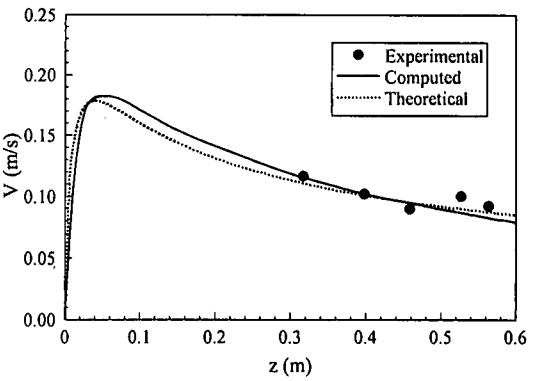

Fig.11 V as a function of z (CASE2)

Figs.6 and **7** show that the computational results of H almost increase linearly with z and the values of H are close to the experimental data and theoretical solution. The calculated value of dH/dz is 0.45.

In **Figs.8** and **9**, average buoyancy B is plotted against z. It is shown that the agreement between computational, experimental and theoretical results is satisfactory. In initial stage the computed B is slightly different from that given by the thermal model. This is because in the thermal model the source is assumed with an elliptic shape of F=0.6 and H_0=0.04m, while in computation the source is a circle with the same value of H_0.

Figs. 10 and **11** present the mass center velocity V as a function of z. It is shown that the motion of the thermal has a fast acceleration and slow deceleration phase. Note that in the theoretical model the thermal shape is assumed as an ellipse with F=0.6, while in the computation it is observed that F slightly increases with distance. This leads a slight difference between computational and theoretical results.

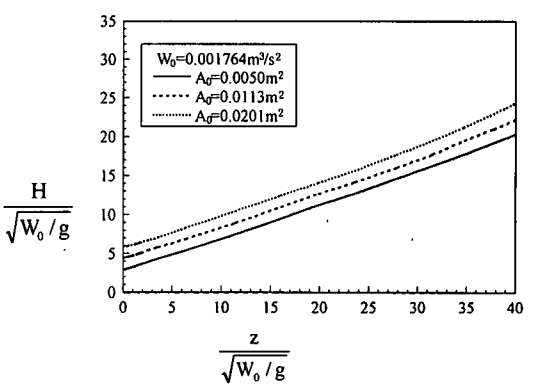

Fig.12 H as a function of z for different A_0

(2) Numerical experiments on the effects of initial conditions

The effects of initial conditions on the motion of thermal are investigated numerically. In the computation the initial total buoyancy has the same value as W_0 =0.001764 m^3/s^2, but the initial volume per unit width A_0 is varied as 0.005, 0.0113 and 0.0201 m^2. The computational results are shown in **Figs.12,13** and **14**, respectively. In the figures, H

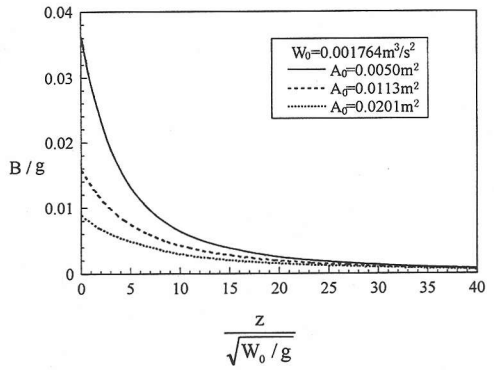

Fig.13 B as a function of z for different A_0

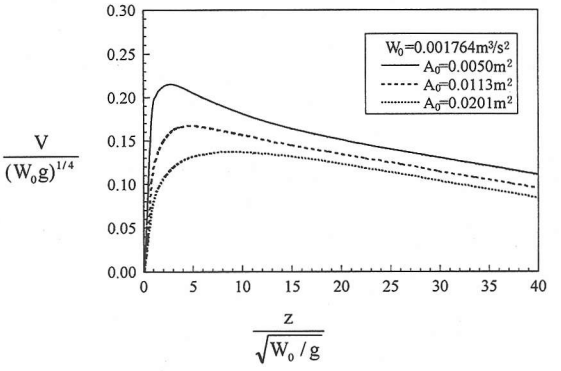

Fig.14 V as a function of z for different A_0

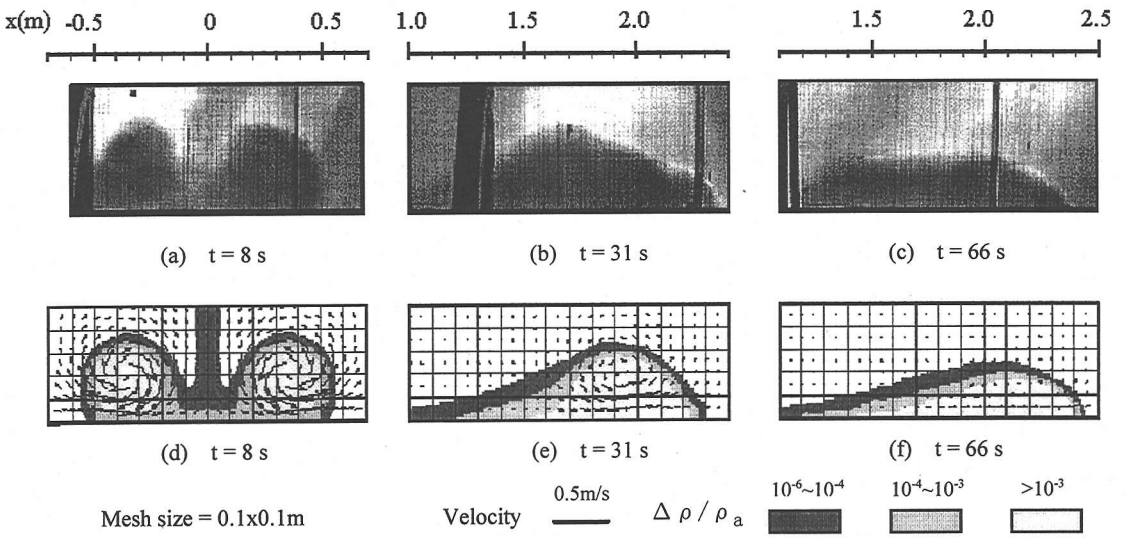

Fig.15 Photographs and computed velocity and density excess fields (CASE2)

and z are non-dimensionalized with $\sqrt{W_0 / g}$, B and V with $(W_0 g)^{1/4}$. It is found that the initial conditions significantly affect the motion of the thermal. Under the same initial total buoyancy, the thermal with larger A_0 has larger width, smaller buoyancy and mass center velocity. The H~z curves for different A_0 almost keep parallel, while the values of B for different A_0 merge to the same value as z increases. The peak values of mass center velocity V decrease evidently as A_0 increases. The thermal with larger A_0 has a smaller acceleration and deceleration than that with smaller A_0.

(3) Horizontal propagation stage

In order to further demonstrate the capability of the present numerical model for simulating complex situations, the motion of a dense cloud subsequently formed after impingement of the thermal on the horizontal bottom boundary is also simulated. The experiments were performed under the same conditions as CASE2, except for water depth = 0.9m. The experimental procedure is the same as the falling stage, except that the average buoyancy B_g for $x_f \geqq 2$m was estimated from the density distribution measured by conductivity meters. In the computation, the domain is 0.9m high and 10.0m long. Initial dense cloud is 2m from left boundary. The imposed boundary conditions for velocity, pressure and density excess are

$$V_\tau = 0 \quad V_n = 0 \quad \text{(bottom boundary)}$$

$$\frac{\partial V_\tau}{\partial n} = 0 \quad \frac{\partial V_n}{\partial n} = 0 \quad \text{(side boundaries)}$$

$$\frac{\partial V_\tau}{\partial n} = 0 \quad V_n = 0 \quad \text{(top boundary)}$$

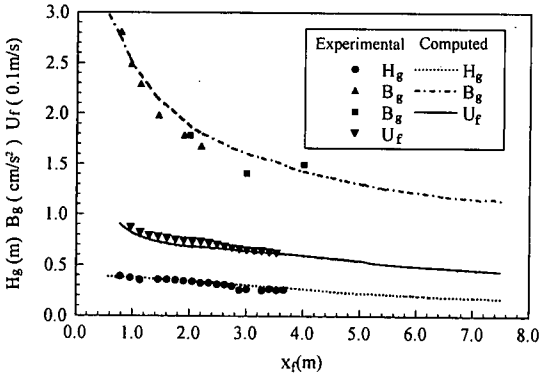

Fig.16 H_g, B_g and U_f as functions of x_f (Data B_g marked with squares are calculated from the density distributions measured by conductivity meters)

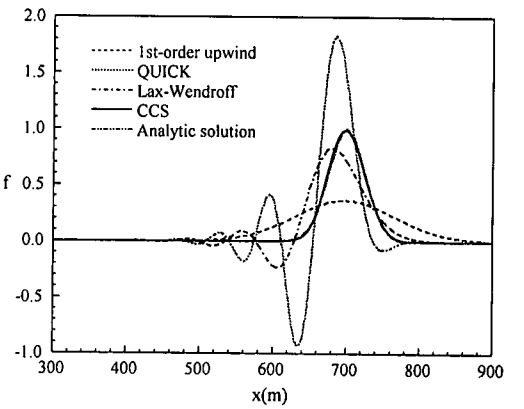

Fig.A-1 Comparison of numerical schemes for 1-D advection problem (t = 500 s)

$$\frac{\partial P}{\partial n}=0 \qquad \frac{\partial \Delta\rho}{\partial n}=0 \qquad \text{(all boundaries)}$$

Other computational conditions and the values of Cs and Scs are the same as those for the falling stage of CASE2.

The horizontal propagation of the dense cloud is illustrated both experimentally and numerically in the photographs and computed density excess distributions in **Fig.15**. The shape, size and propagation speed of the cloud are well predicted. In **Fig.16**, the computed results of height H_g, average buoyancy B_g and front propagation speed U_f of the dense cloud are quantitatively compared with the experimental results, where x_f is the horizontal distance measured from the center of initial dense cloud to the front of horizontally propagating cloud. H_g and U_f are predicted quite accurately. The fairly good agreement between predicted and experimental B_g is achieved.

5. CONCLUSIONS

The whole process of a dense cloud instantaneously released into a less dense fluid with finite depth is investigated experimentally and numerically. The following conclusions are obtained.

(1) The comparisons of computational results of main flow characteristics, including shape, size, mass center velocity and average buoyancy, with the experimental and theoretical results show that the numerical simulation gives a good description of the thermal, when the Smagorinsky constant Cs=0.16 and the subgrid turbulent Schmidt number Scs=0.1.

(2) The comparisons between computational and experimental results of height, average buoyancy and propagation speed also show that the motion of a dense cloud subsequently formed after impingement of the thermal on the horizontal bottom boundary is well predicted using the same values of Cs and Scs as those for falling stage.

(3) The added mass coefficient A_m and drag coefficient C_d in the thermal model are determined as 0.6 and 0.8, respectively, based on the numerical simulation. The computational results confirm that the value of the entrainment coefficient E_d is nearly independent of distance and the average value of E_d is about 0.4.

ACKNOWLEDGEMENT: This study was supported by the Grant-in-Aid for Science Research (B) of the Ministry of Education and Culture, Japan, under the Grant No.08455232.

APPENDIX A COMPARISONS BETWEEN CCS SCHEME AND SOME CONVETIONAL SCHEMES

The comparisons between the CCS scheme and some conventional schemes are made by advecting a Gaussian profile

$$f(x)=\exp\left(-\frac{(x-x_0)^2}{2\sigma_0^2}\right)$$

Computational conditions are as follows: $x_0 = 200\,\text{m}$, $\sigma_0 = 25\,\text{m}$, velocity $U = 1\,\text{m/s}$, space step size $\Delta x = 10\,\text{m}$, time step size $\Delta t = 2\,\text{s}$, and Courant number $Cr = \Delta tU/\Delta x = 0.2$. **Fig.A-1** shows that the CCS scheme yields much better result than other three schemes.

The CCS scheme for 2-D advection problems is investigated by advecting a Gaussian hill (**Fig.A-2**) with initial concentration distribution

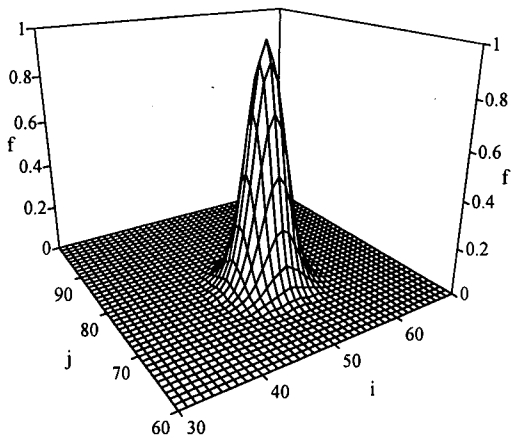

Fig.A-2 Initial distribution for 2-D advection problem

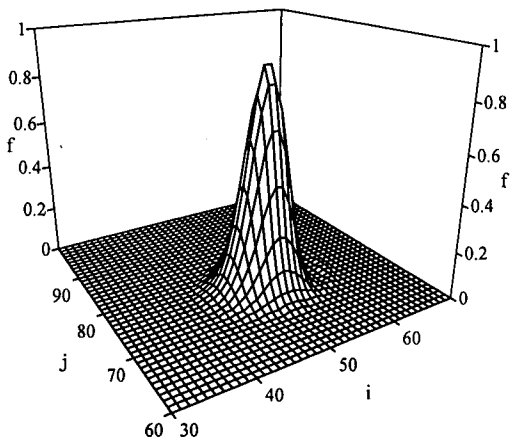

Fig.A-3 Computational result by CCS

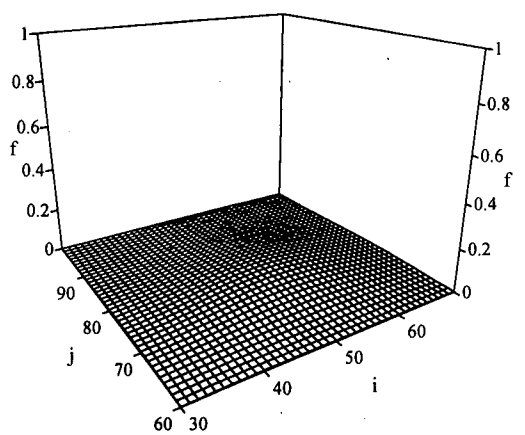

Fig.A-4 Computational result by 1st-order upwind scheme

$$f(x,y)=\exp\left(-\frac{(x-x_c)^2+(y-y_c)^2}{2\sigma_0^2}\right)$$

where (x_c, y_c) are the coordinate of initial concentration distribution center. The steady rotational flow field is $U_1=-\omega(y-y_0)$ and $U_2=\omega(x-x_0)$, where ω is an angular velocity in radians/sec and (x_0, y_0) is the axis of rotation. In particular, $x_c=500\,m$, $y_c=750\,m$, σ_0=25m. $x_0=500\,m$, $y_0=500\,m$ and $\omega=2\pi/628$. The computational domain is a square with 100×100 cells. The space step size $\triangle x=\triangle y=10$ m. The time step size $\triangle t=1$ s. The numerical solutions after one revolution (t=628 s) by the CCS scheme and the first-order upwind scheme are shown in **Figs. A-3** and **A-4**, respectively. It is seen from these figures that the CCS scheme is nearly free from numerical diffusion and numerical oscillation, while the result by the first-order upwind scheme is very diffusive.

REFERENCES

1) Scorer, R.S.: Experiments on convection of isolated masses of buoyant fluid, J. Fluid Mech., Vol.2, pp.583-594, 1957.
2) Wang, C.P.: Motion of a turbulent buoyant thermal in a calm stably stratified atmosphere, *The Physics of Fluids*, Vol.16, pp.744-749, No.6, 1973.
3) Escudier, M.P. and Maxworthy, T.: On the motion of turbulent thermals, *J. Fluid Mech.*, Vol.61, part 3, pp.541-552, 1973.
4) Baines, W.D. and Hopfinger, E.J.: Thermals with large density difference, *Atmospheric Environment*, Vol.18, No.6, pp.1051-1057, 1984.
5) Akiyama, J., Ura, M., Ying, X., Imamiya, M. and Suyama, M.: Flow characteristics of dense cloud instantaneously released into quiescent fluid, *Annual Journal of Hydraulic Engineering*, JSCE, Vol.42, pp.529-534, 1998 (in Japanese).
6) Nakatsuji, K., Tamai, M. and Murota, A., Dynamic behaviors of sand clouds in water, *Int. Conf. Phys. Modelling of Transport and Dispersion*, M.I.T. Boston, 8C.1-8C.6, 1990.
7) Tamai, M., Muraoka, K., Murota, A. and Machida, H.: Study on initial stage of diffusion process of turbidity in direct dumping of soil, *Journal of Hydraulic, Coastal and Environmental Engineering*, JSCE, No.515/II-31, pp.77-86, 1995
8) Li, C.W.: Convection of particle thermals, *Journal of Hydraulic Research*, Vol.35, No.3, pp.363-376, 1997.
9) Tamai, M. and Muraoka, K.: Numerical simulation on characteristics of turbidity transport generated in direct dumping of soil, *Annual Journal of Hydraulic Engineering*, JSCE, Vol.42, pp.541-546, 1998 (in Japanese).

10) Oda, K., Shigematsu, T. Onishi, N. and Inoue, M.: Numerical simulation of settling and spreading behavior of particle cloud using improved DEMAC method, *Proceedings of Coastal Engineering*, JSCE, Vol.39, 1992
11) Paolucci, S. : Direct numerical simulation of two-dimensional turbulent natural convection in an enclosed cavity, *J. Fluid Mech.*, Vol.215,pp.229-262,1990
12) Tafti D.K. and Vanka S.P. : A numerical study of flow separation and reattachment on a blunt plate, *Phys. Fluids*, A3(7), pp.1749-1759, July 1991
13) Fang F.M. Hiseh, W.D., Jong, S.W., and She, J.J. : Unsteady turbulent flow past solid fence, *J. Hydraulic Engineering*, Vol.123, No.6, pp.560-565, June, 1997
14) Eidson, T. M. : Numerical simulation of the turbulent Rayleigh-Benard problem using subggrid modelling, *J.Fluid Mech.*, Vol.158, pp.245-268, 1985
15) Holly, F.M. and Preissmann, A.: Accurate calculation of transport in two dimensions, *Journal of Hydraulics Divisions*, ASCE, Vol.103, pp. 1259-1277, 1977.
16) Ding, D. and Liu, P.L.F.: An operator-splitting algorithm for two-dimensional convection-dispersion-reaction problems, *International Journal of Numerical Method in Engineering*, Vol.28, pp.1023-1047, 1989.
17) Ahlberg, J.H., Nilson,E.N. and Walsh, J.L.: The theory of splines and their applications, Academic Press, New York, 1976.
18) Ying, X., Akiyama, J. and Ura, M.: Numerical study of 2-D inclined starting plumes using LES, *Journal of Hydroscience and Hydraulic Engineering*, JSCE, Vol.17, No.1, pp.117-129, 1999.

(Received October 19, 1998)

有限な水深を有する静水中に直投された重い流体の挙動に関する研究

応　新亜・秋山　壽一郎・浦　勝

有限な水深を有する静水中に直投された重い流体塊の落下挙動，さらにはその底面衝突から水平流動に至る一連のプロセスについて実験的・数値的に論じた．浮力効果を考慮した修正Smagorinskyモデルに基づくLESと１流体モデルに基づく数値モデルを新たに構築した．落下挙動について抗力項を考慮したサーマル理論と実験値を用いてモデル定数を同定した上で，底面衝突から水平流動に至る複雑な流体塊の流動状況が落下挙動と同じモデル定数を用いて精度良くシミュレートできることを定量的に示した．